Applied Surface Science 449 (2018) 745–754

Contents lists available at ScienceDirect

Applied Surface Science

journal homepage: www.elsevier.com/locate/apsusc

Full Length Article

Studies on biodegradable polyurethane-SWCNTs nanocomposite films by covalent approach: Physicochemical, electric and mechanical properties

Senthil A. Gurusamy Thangavelu[a,*], Adhigan Murali[b], Madhurakkod Sharanya[a,b], Sellamuthu N. Jaisankar[b], Asit Baran Mandal[b,*]

[a] SRM Research Institute and Department of Chemistry, SRM University, Kattankulathur, 603203 Tamil Nadu, India
[b] Polymer Division, Council of Scientific and Industrial Research-CLRI, Adyar, Chennai, 600020 Tamil Nadu, India

ARTICLE INFO

Article history:
Received 2 November 2017
Received in revised form 23 January 2018
Accepted 29 January 2018
Available online 8 February 2018

Keywords:
Biodegradable nanocomposite films
Functionalized carbon nanotubes
Covalent approach
Impedance measurement
Thermal stability
Tensile strength

ABSTRACT

Biodegradable control polyurethane (PU) film as well as PU nanocomposite films (PU-SWCNTs), covalently incorporated with minor amount of hydroxyl single walled carbon nanotubes [$(OH)_n$-SWCNTs] have been formulated to investigate the influence of SWCNTs on the matrix of PU (3-dimensional network of soft and hard segments). Biodegradable polyol, polycaprolactone triol (PCL, ~70%), diisocyanate (TDI, ~21%) and 1, 4- butane diol (BDO) as chain extender were taken to react at 70 °C under inert atmosphere in the presence of amine catalyst (PMDETA) *via* prepolymer process to obtain the control PU film by casting approach, whereas *in situ* addition of $(OH)_n$-SWCNTs into the above formulation can afford the covalently incorporated PU-SWCNTs films by the identical protocol. PU and PU-SWCNTs films loaded with variable quantity of $(OH)_n$-SWCNTs (0.01, 0.03, 0.05, 0.1 and 0.3 wt.%) were characterized to identify the enhancement of their physicochemical properties such as optical, electrical conductivity, thermal and mechanical properties. These film samples were characterized by FT-IR, Raman, ATR-FT IR, UV–vis DRS, solid state ^{13}C NMR, XRD, impedance measurements, DSC, TGA, EDX, SEM, AFM, optical microscope and tensile strength data.

1. Introduction

Polymeric nanocomposites use to constitute the homogeneously dispersed organic or inorganic nanomaterial on polymer matrix with variable loading in the range of 0.5–10% [1]. Both bio-derived and biodegradable polymer matrices have intrigued researchers due to the depletion of fossil resources, used as monomers for the wide range of synthetic polymers [2–4]. Polymeric products like polypropylene, polystyrene, polyethylene and polymethylmethacrylate are accumulated as non-biodegradable wastes globally including variety of composites [5]. Since the biodegradable polymers are formulated alternatively from the renewable and biodegradable precursors, polymeric nanocomposites derived from this category of samples have to be tuned in terms of mechanical, electrical and thermal properties, these properties are possible to achieve conventionally in nanocomposites of commonly available non-biodegradable polymers [6,7].

PU and PU nanocomposites can be developed by the versatile synthetic methodologies as environmental friendly process upon elimination of toxic chemicals and multi-step procedure to develop the potential products possessing the desirable biological, physicochemical, mechanical and conductive properties. These products are under investigation for the various applications like energy harvesting, self-healing, shape memory and tissue engineering. Aliphatic polyester, polycaprolactone polyol (polycaprolactone diol and polycaprolactone triol) is classified as one of the essential biodegradable precursor to replace the role of non-degradable petrochemicals, their degraded by-products use to be non-toxic [8–12]. Synthesis of PU from polycaprolactone diol or PCL found to be desirable for their properties like biodegradable, hydrophobic, biocompatible and bioresorbable due to their feasible conversion into mild products. For *e.g.*, 6-hydroxyhexanoic acid can be converted into natural metabolite, adipic acid by microsomal ω-oxidation [13,14]. We are aiming to develop the biodegradable nanocomposite as film (~1.5 mm) with characteristic properties from the petro-based precursor (trifunctional polyol, PCL) to for-

* Corresponding authors.
E-mail addresses: senthilandavan.t@ktr.srmuniv.ac.in (S.A. Gurusamy Thangavelu), abmandal@hotmail.com (A.B. Mandal).

https://doi.org/10.1016/j.apsusc.2018.01.275
0169-4332/

mulate PU as well as PU nanocomposite in the form of films, loaded with trace quantity of carbonaceous nanomaterial (SWCNTs) by casting method for the investigation of their optical, thermal, mechanical and conductivity properties [15–17].

Essentially, polycaprolactone diol ($f_n = 2$) has been explored by the several groups, whereas the PCL ($f_n = 3$) found to be chosen as the polyol precursor in limited cases for our knowledge. PU scaffold from the mixture of polycaprolactone diol and PCL *via* one-shot method is found to be an alternative for the cartilaginous tissue in plastic and reconstructive surgery [18–20]. In the present work, PCL is used as major component (~70%) for the development of biodegradable nanocomposite film with hydroxyl functionalized SWCNTs. In this formulation, hard segment of PU matrix is comprised of urethane link from the highly reactive aromatic diisocyanate (TDI) while the soft segment is associated with aliphatic polyester polyol (PCL, ~M.W. 2000).

Inorganic carbon nanotubes use to be exemplified as ubiquitous and subject of interest since their discovery in 1991 by Iijima [21]. Both pristine SWCNTs and functionalized SWCNTs in the form of nanomaterials tend to be utilized in variety of applications, nanoelectronics to nanocomposite fabrication due to its high aspect ratio with thermal, mechanical and electronic properties [22]. As such SWCNTs can exhibit enormous potential to explore the enhancement of fore mentioned properties, even upon loading well below 0.5% in polymers matrix [23,24]. It is typical to form polymer nanocomposites based on SWCNTs for several applications, by the versatile of methods such as *in situ* polymerization, non-covalent, solution, grafting and melt mixing etc.[25–29]. Among those methods, Song and Hesheng et al. have preferred to accomplish the formulation of PU nanocomposites using SWCNTs by two step *in situ* polymerization [30,31]. Since few challenges are accounted with SWNTs such as poor miscibility with polymer and solvents, both solution processing and the preparation of composite samples containing carbon nanotubes (CNTs) found to be uncommon. In fact the chemical functionalization of CNTs has been a subject of several reviews, wherein the solubility, dispersion and stress transfer were demonstrated to illustrate the mechanical properties [26–28]. The facile interface between SWCNTs and polymer matrix enhances the load transfer among the nanotubes and polymer network to exclude interfacial collapse, particularly the functionalized SWCNTs tend to be affordable to form such robust polymer composites. Chemical functionalization favours the isolation of entangled or bundled SWCNTs for the suitable orientation.

Another concern about the polymer nanocomposite is identified that if SWCNTs gathered by agglomeration, which could cause the loss of inherent properties supposed to be incorporated into the 3-dimensional network of polymer matrix. To ascertain the uniform distribution of SWCNTs on polymer matrix, we have established an efficient and viable strategy to accomplish the effective interfacial adherence of functionalized $(OH)_n$-SWCNTs with polymer matrix *via* covalent bond [32–34]. In general, functionalization of SWCNTs requires the treatment of hazardous reagents and stringent reaction conditions with multi-step synthetic route to obtain the poor yield of functionalized SWCNTs [35–38]. Carboxyl and hydroxyl functional groups were substituted on carbon nanotubes by simple mechanical grinding of the reactants at ambient condition by mechano-chemical reaction [39,40].Our two steps synthetic strategy to substitute hydroxyl groups on side walls of SWCNTs to obtain good yield of $(OH)_n$-SWCNTs has excluded any multi-step or rigorous condition during the reaction, which can retain the unique properties of SWCNTs as well [32].

At present, PU nanocomposite formulated in this work is described to be unique due to the fact that the biodegradable trifunctional polyol, PCL has been chosen to form prepolymer followed by covalent incorporation with $(OH)_n$-SWCNTs in the presence of chain extender (BDO). In literature, reports to develop the polymeric nanocomposites with biodegradable properties exist under progress to match with the properties of conventionally available non-biodegradable polymers. Moreover, our report demonstrate the efficient and fairly cost effective use of trace quantity (0.01–0.3 wt.%) of $(OH)_n$-SWCNTs in the formulation of PU-SWCNTs nanocomposite in the form of film (~1.5 mm). In general, PU-SWCNTs nanocomposite film formulations use to encounter the opportunity to exhibit agglomeration of SWCNTs while used as pristine sample (*p*-SWCNTs). Currently, *in situ* addition to incorporate the functionalized $(OH)_n$-SWCNTs towards the generation of covalent bond across the network of PU matrix can exclude the possibility of agglomeration and improves the opportunity of effective interfacial interaction and preferred homogeneous distribution of SWCNTs on the film of PU network.

2. Experimental details

2.1. Materials

Polycaprolactone triol (PCL, CAPA 3201, ~M.W. 2000, soft waxy solid at RT, OH value: 85.85, melting point: 40–50 °C) has been received as the gift sample from Perstrop India Limited. *Pristine* SWCNTs, 2, 4-toluene diisocyanate (TDI), 1, 4-butanediol (BDO), N, N, N', N", N"-pentamethyldiethylenetriamine (PMDETA) and dry toluene were procured from Sigma Aldrich, USA. Tetrahydrofuran was purchased from Merck specialties Private Limited and distilled after stored overnight in calcium chloride. The other reagents were procured from the chemical suppliers available at India.

2.2. Methods

Tensile strength and Youngs moduli were measured using an Instron 3369 tensile testing system, USA. ABB MB3000 spectrometer was used to collect ATR-IR on control PU and nanocomposite films. Raman spectra for the functionalized SWCNTs and nanocomposite films were collected from the Confocal Raman spectrometer (Nanophoton Corporation, Japan, excited at 532 nm). AFM imaging was carried out by NT-MDT (NTEGRA Prima, Netherlands). UV–vis DRS data was characterized using a LAMBDA 650 UV/*vis* spectrophotometer. OLYMPUS BX50 with transmitted light was used to record the optical microscopic images of nanocomposite films. DSC profiles were recorded between ambient temperature to 300 °C using TA-Instruments DSC Q200. TGA thermogram for the samples was carried out by Q50 TGA, TA Instruments. XRD pattern of PU was studied by X-ray diffraction analysis by X-ray diffractometer (Rigaku miniflex). The probe sonicator Sonics VCX 750 (750 W, 20 KHz, Sonics & materials, Inc., Newtown, USA) operated at 60% amplitude to get homogeneous material.

2.3. Control PU film

PCL (4 g) was taken in three necked RB flask, melted at 50 °C in oil bath and allowed to stir using mechanical stirrer under nitrogen atmosphere for 15 min under inert atmosphere. PCL and 2, 4 – toluene diisocyanate (TDI) were taken in 1:2 ratio to obtain prepolymers. TDI (1.20 ml) was then added and continued to stir at the temperature in oil bath. After 10 min, dry THF (10 ml) and tertiary amine, PMDETA (1.26 μl) were added to polyol. The reaction temperature was raised to 75 °C and stirred constantly for 90 min. In the mean while reaction mixture was added occasionally with THF (3 ml) to maintain its viscous state as well as to avoid the gel formation. Now, the chain extender (1, 4-butane diol, 60 μl) was added and continued to stir for 15 min. The viscous reaction mixture was removed from the oil bath and the composition was transferred to a petri dish. The curing step was carried at ambient temperature for a week followed by curing at 75 °C under vacuum for 6 h. After

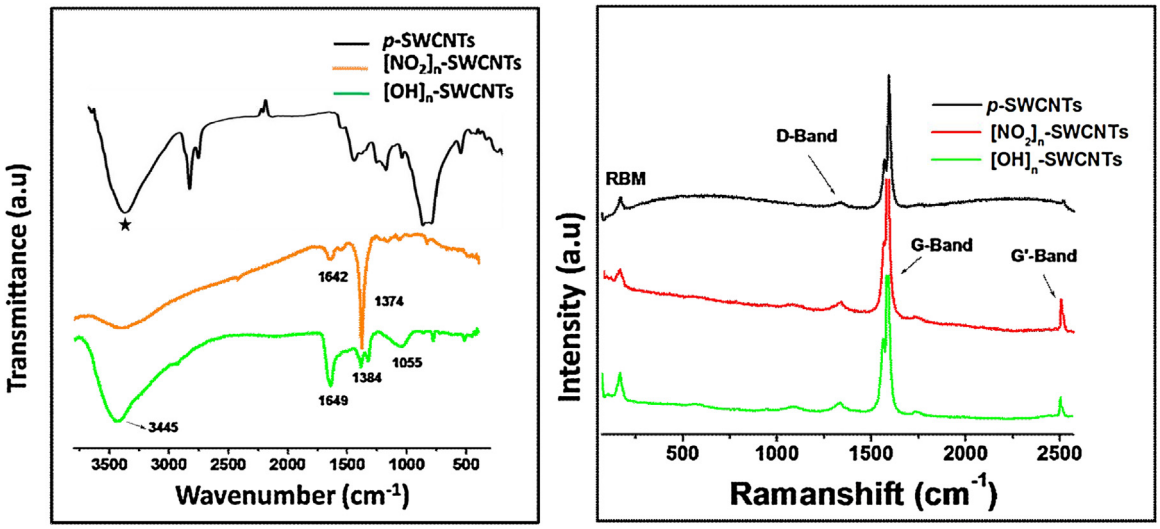

Fig. 1. (a) FT IR spectra of *p*-SWCNTs (⋆denotes moisture in KBr pellet), $(NO_2)_n$-SWCNTs and $(OH)_n$-SWCNTs, (b) Raman spectra of *p*-SWCNTs, $(NO_2)_n$-SWCNTs and $(OH)_n$-SWCNTs.

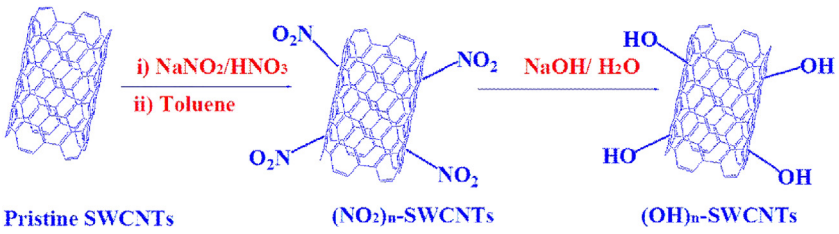

Scheme 1. Functionalization of SWCNTs *via* two step synthetic route by mild reagent/condition.

curing, the PU film was used for the measurement of data during various characterizations.

2.4. PU-SWCNTs nanocomposite films

PU-SWCNTs nanocomposites were prepared from the viscous state of PU prepolymer obtained from the reaction of PCL, TDI and PMDETA for 2 h as per the procedure described for the control PU. Further reaction of prepolymer with chain extender (1, 4-butane diol, 60 μl) for 5 min was conducted at 75 °C in the same RB flask. To the above reaction mixture, suspension of $[OH]_n$-SWCNTs (0.021 g, 0.3 wt.%, after sonication for 15 min) in dry THF (10 ml) was added and stirred for 30 min at 75 °C. PU nanocomposite appeared to be grey in color after the reaction of SWCNTs and removed from oil bath to transfer uniformly under hot condition on glass petri dish. To recover the film, curing process carried out at ambient temperature for a week and then curing at 75 °C under vacuum for 6 h. Moreover, the identical procedure was adopted to obtain the other nanocomposite films upon $[OH]_n$-SWCNTs loadings, 0.007 g (0.1 wt.%), 0.0035 g (0.05 wt.%), 0.0014 g (0.03 wt.%) and 0.0007 g (0.01 wt.%).

3. Results and discussion

3.1. Synthesis of hydroxyl single walled carbon nanotubes [$(OH)_n$-SWCNTs]from p-SWCNTs

Synthesis of $(OH)_n$-SWCNTs from *p*-SWCNTs is occurred to be non-trivial and daunting task to functionalize on the side walls of *p*-SWCNTs due to its lack of solubility or dispersion and need of rigorous condition using vigorous reagents to obtain the poor yield of product. We have recently reported the functionalization of hydroxyl group on side walls of SWCNTs by adopting simple and mild route for the conversion of fullerenols from fullerenes [32].

The above synthesis has been succeeded by the generation of reddish brown nitro radical from the mixture of concentrated nitric acid and sodium nitrite and immediate reaction with the suspension of *p*-SWCNTs in toluene afforded $(NO_2)_n$-SWCNTs. Further conversion into $(OH)_n$-SWCNTs was accomplished quantitatively by the hydrolysis of $(NO_2)_n$-SWCNTs under alkaline medium (3N, NaOH) for 4 h at 50 °C followed by precipitation using methanol (MeOH) to obtain the product in good yield (~70%). Both stepwise products from the chemical functionalization steps are characterized by FT IR and Raman data as depicted in Fig. 1.

3.1.1. FT IR and Raman data of functionalized single walled carbon nanotubes [$(OH)_n$-SWCNTs]

The products obtained from step I and II of Scheme 1 have been characterized by FT IR and Raman data. As shown in FT IR data of Fig. 1, $(NO_2)_n$-SWCNTs use to exhibit characteristic vibrational frequencies as compared to *p*-SWCNTs, supported the substitution of $-NO_2$ groups on side wall of SWCNTs. As such vibrational frequency of *p*-SWCNTs at 1642 cm^{-1} is attributed to the —C=C— stretching of its structure and signal at 1055 cm^{-1} arisen due to —C—C— stretching of cyclic units in SWCNTs, whereas the broad peak around the region of 3350–3450 cm^{-1} occurred due to the moisture present in the KBr pellet. In addition to the signals stated for *p*-SWCNTs, characteristic peak at 1374 cm^{-1} has been noticed for the $(NO_2)_n$-SWCNTs. Further, $-NO_2$ functional group of SWCNTs was subjected to hydrolysis to afford $(OH)_n$-SWCNTs is evidenced by the new signal with respect to —OH group at 3445 cm^{-1} and peak at 1374 cm^{-1} got disappeared as inferred in Scheme 1 [32,37,41].

Moreover, Raman spectra provided the strong evidence for the transformation of *p*-SWCNTs in the consecutive steps (Scheme 1).

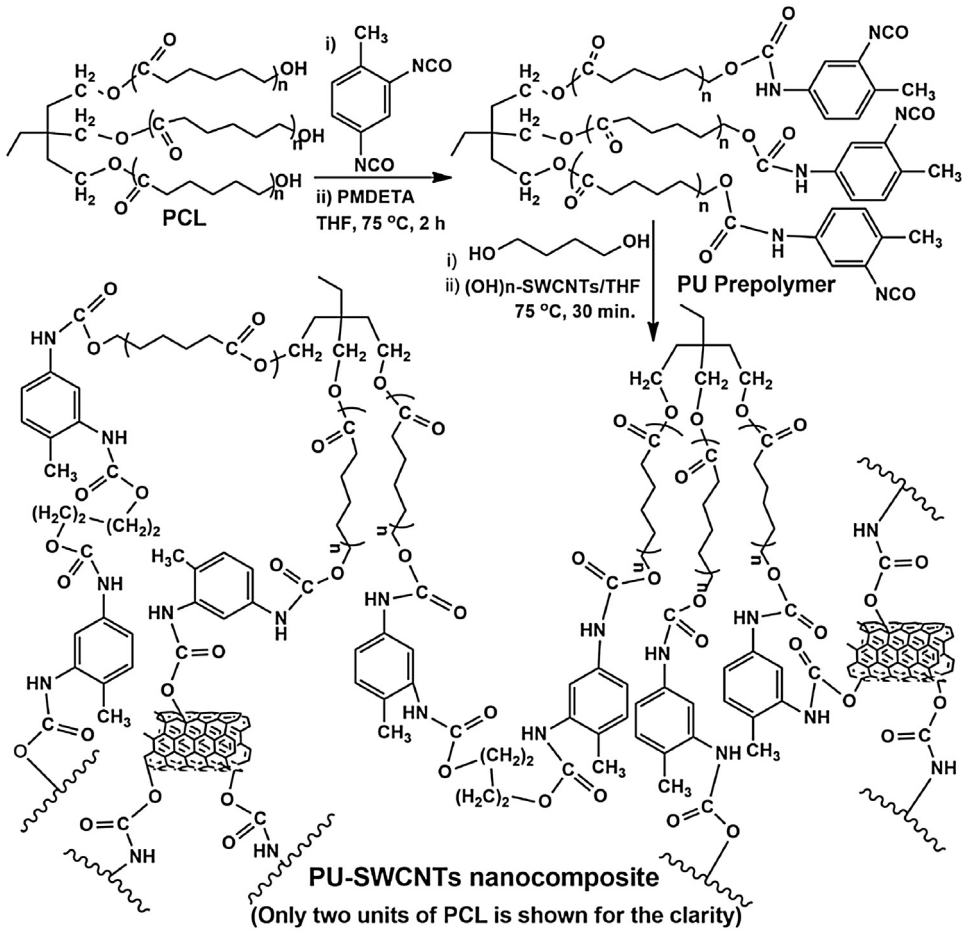

Scheme 2. Synthetic formulation of PU control and PU nanocomposite samples with variable loading of $(OH)_n$-SWCNTs to incorporate SWCNTs via covalent bond into PU matrix.

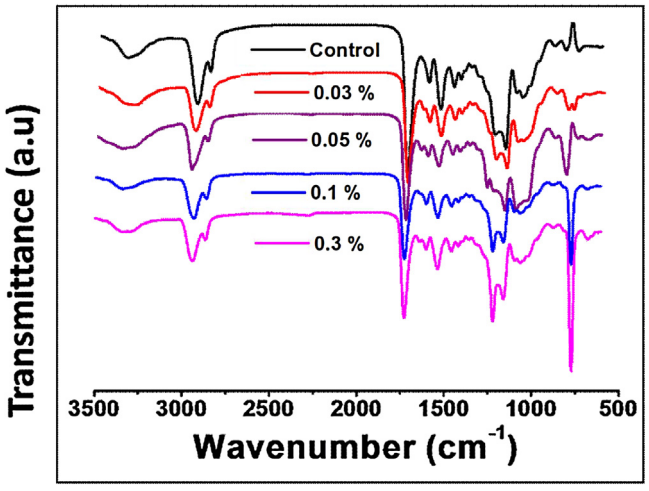

Fig. 2. ATR-IR of control and PU-nanocomposites films.

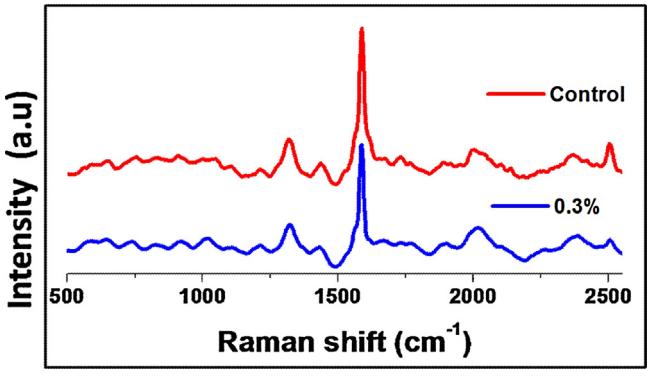

Fig. 3. Raman spectra of control PU and PU nanocomposite (0.3 wt.%).

Despite the RBM value of *p*-SWCNTs around 167–301 cm^{-1} was reported to vary according to the synthetic approach, herein found to observe at 167 cm^{-1} for this sample in Fig. 1. Raman allowed G-mode has arisen at 1586 cm^{-1} for *p*-SWCNTs due to the addition of six high energy tangential modes based on breaking of symmetry of tangential vibration in graphene sheet. The characteristic Raman feature of SWCNTs for the disorder-induced D-mode occurred to detect at 1333 cm^{-1} and the respective second order harmonic band appeared as the G'-band at 2504 cm^{-1}. The intensity of the D-band of $(NO_2)_n$-SWCNTs found to improve slightly due to the substitution of side wall of SWCNTs and consequently the respective second harmonic band, G' at 2504 cm^{-1} also increased accordingly. The identical trend was identified in observed values of D and G' with case of final product, $(OH)_n$-SWCNTs, it corroborated the substitution on side wall of SWCNTs [32,37,42].

3.2. Synthesis of PU and PU nanocomposite films

As such the schematic representation of PU-SWCNTs nanocmposites formulation in Scheme 2 has been implemented with

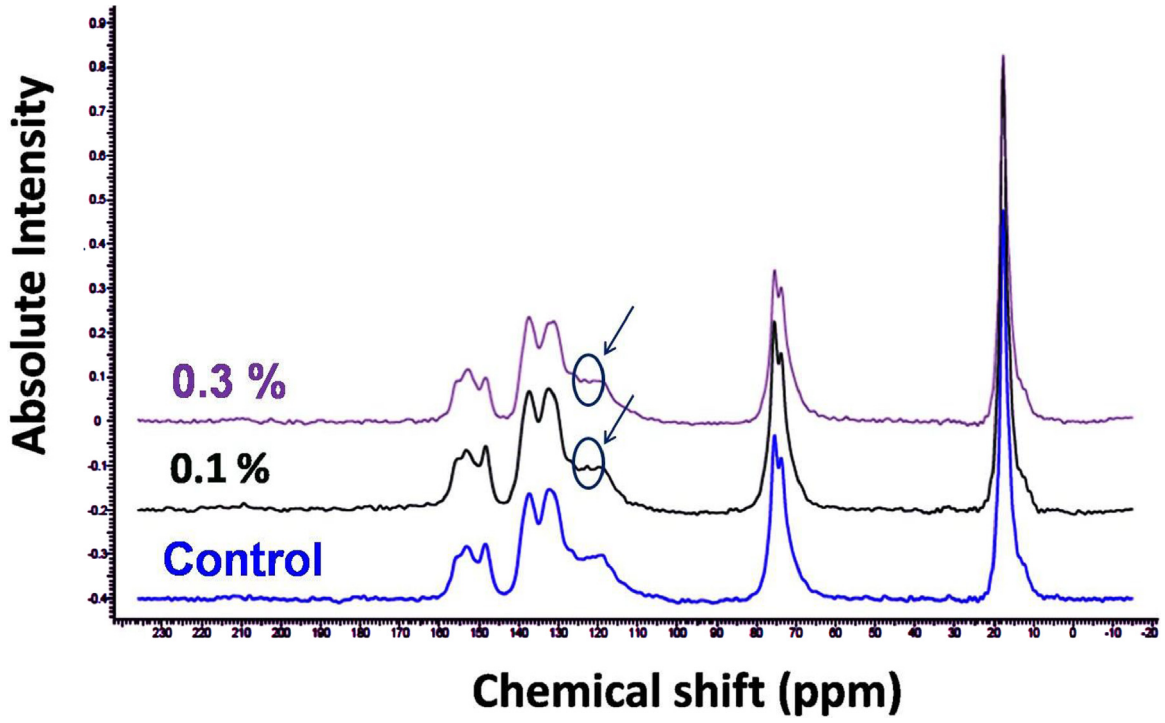

Fig. 4. Solid state ^{13}C NMR data of PU and PU nanocomposite films.

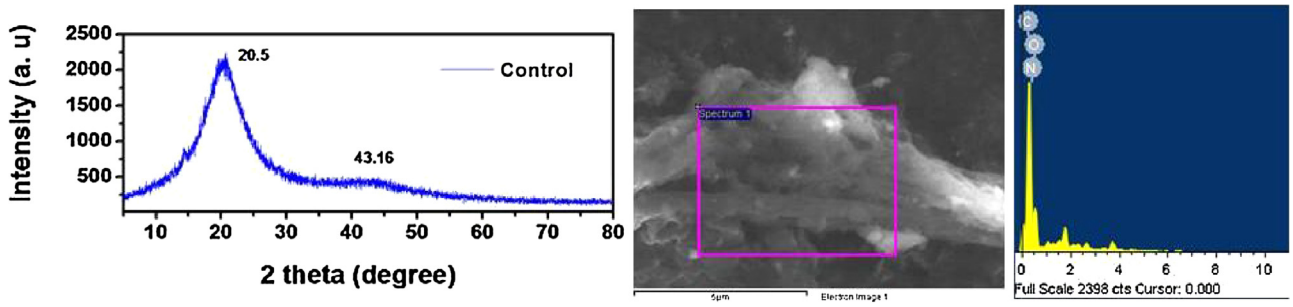

Fig. 5. XRD and EDX data for the PU film sample.

suitable catalyst to enhance the reactivity of mild reactive polyol, PCL in the presence of tertiary amine (PMDETA) with highly reactive TDI.

PMDETA employed as suitable catalyst to succeed the reaction of PCL (CAPA3201) with TDI to form prepolymer under inert atmosphere at 75 °C followed by reaction with the chain extender (BDO) in THF medium to afford PU matrix. *In situ* addition of $(OH)_n$-SWCNTs reacted with PU to form covalently attached nanocomposites. The viscous medium has been transferred to petri dish to recover the films after curing process. These film samples of PU and PU-SWCNTs with different loading have been characterized primarily by vibrational spectra as shown in Fig. 2.

3.2.1. *Vibrational spectral data of PU and PU-SWCNTs nanocomposite film samples*

ATR-IR data shown for these film samples in Fig. 2 supported the complete reaction of isocyanate and hydroxyl groups to form urethane link in PU of each film sample, the vibrational frequency at 3350 cm^{-1} inferred the axial stretching vibration of −NH group and signal at 2938 cm^{-1} detected the —C—H stretching vibration of $-CH_2$ group. The existence of hydrogen bond through —C═O group of urethane linkage can be determined by identifying the peak position at 1700 cm^{-1} for the hydrogen bonded —C═O groups, while free —C═O groups use to appear at 1726 cm^{-1}. Since such hydrogen bonds did not arise with these samples, no peak was noticed at 1700 cm^{-1}. The peak at 1560 cm^{-1} inferred the N—H bending vibration of urethane bond and peak at 1240 cm^{-1} represented the stretching vibration of —C—N group of urethane link. The intense peak appeared at 1190 cm^{-1} due to C—O—C vibration frequency, based on molecular skeleton of PCL. Aromatic ring stretch found to appear at 1592 cm^{-1} and aromatic out of plane bend frequency was identified at 772 cm^{-1} [8,20].

In addition to the Raman spectral feature of *p*-SWCNTs and $(OH)_n$-SWCNTs depicted in Fig. 1, samples of PU and PU nanocomposite loaded with 0.3 wt.% of SWCNTs are shown in Fig. 3. In the study of analogous report on PU-SWCNTs by Song coworkers, peaks correspond to SWCNTs viewed evidently and shift in positions noticed upon loading 2.0 wt.%, while loading range varied between 0.5–2.0 wt.% [30,31]. In Fig. 3, Raman spectra found to show identical peaks pattern wherein no appreciable intensity of SWCNTs peaks or shift. This is due to the less quantity loading of SWCNTs (0.3 wt.%). PU structural network has represented the existence of aromatic TDI and urethane linkage consist of different functional groups based on amide I (1720 cm^{-1}), amide-II (1538 cm^{-1}) and amide-III (1533 cm^{-1}) and 1619 cm^{-1}, some of those peaks merged together as broad peak [43,44]. Altogether Raman data found to

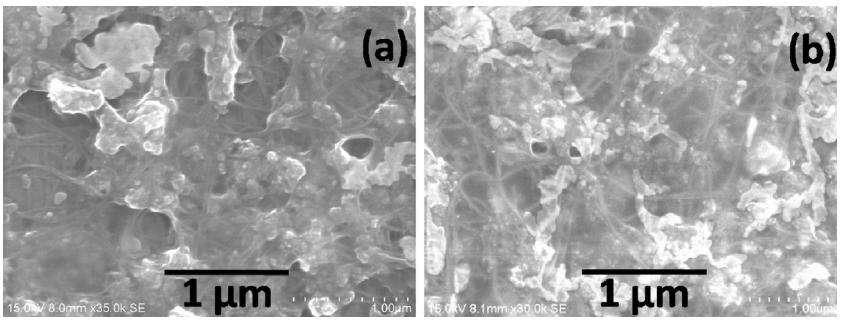

Fig. 6. FESEM image of SWCNTs distribution on PU nanocomposite films.

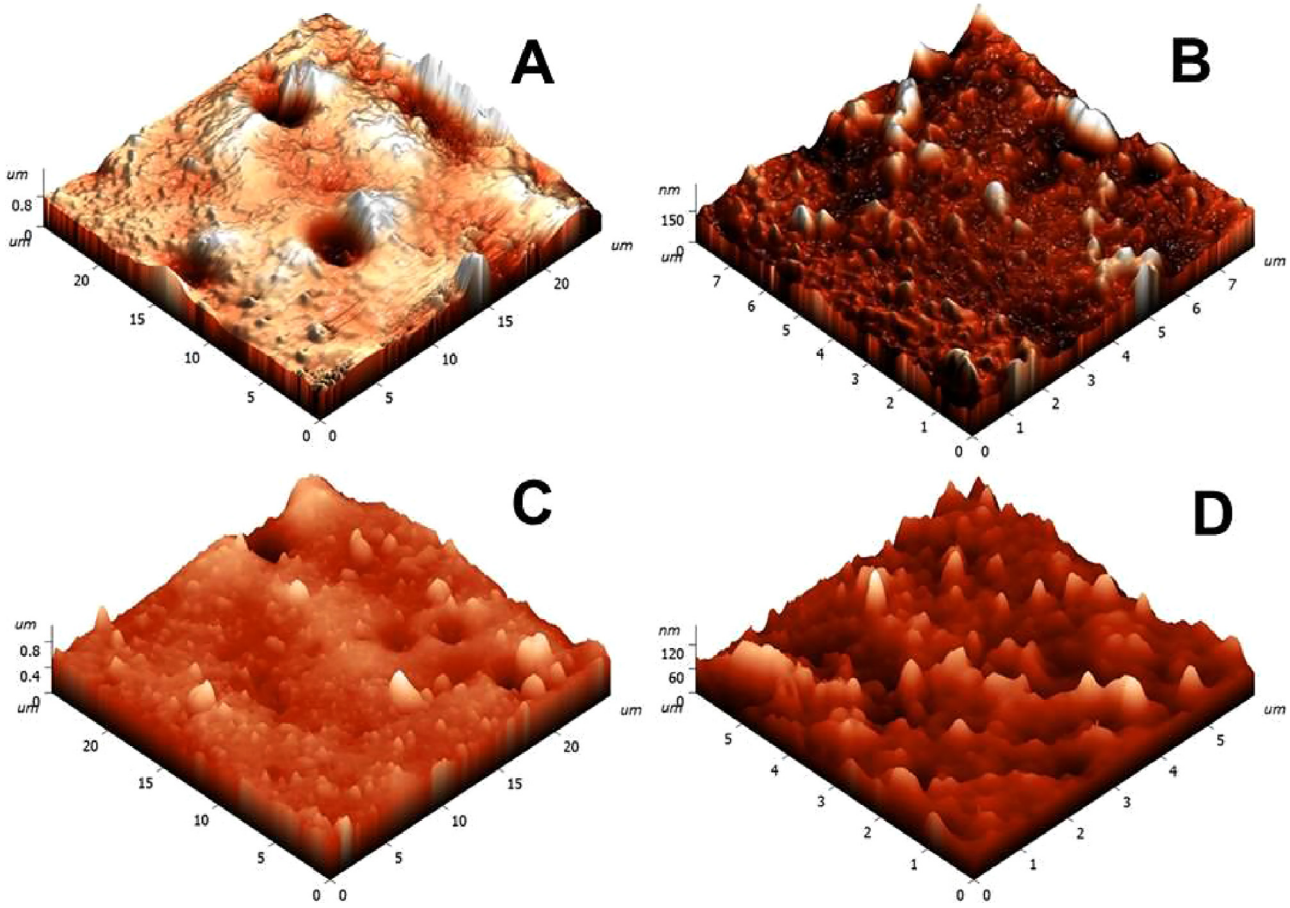

Fig. 7. Three dimensional AFM images [A ($25 \times 25\ \mu m^2$), B ($8 \times 8\ \mu m^2$), C ($25 \times 25\ \mu m^2$) and D ($6 \times 6\ \mu m^2$)] collected at different regions of PU-SWCNTs nanocomposite (0.3 wt.%).

support the interaction of SWCNTs with PU to form covalent bond [8,14,20].

3.2.2. Structural characterization to determine PU and PU-SWCNT

Since these film samples are insoluble in organic solvents even under hot condition, it was chosen to characterize these film samples alternatively by solid state NMR data as shown in Fig. 4. In case of sample preparation, film samples were cut into finite pieces and grinded with dry KBr solid using mortar and pestle to collect ^{13}C NMR data. TDI containing isocyanate groups at 2 and 4 and positions of benzene ring tend to react at variable rate to afford urethane bonds, generated the corresponding NMR signals to develop as broad signal in the down field region, 147–158 ppm. Methyl group of TDI has merged with aliphatic region of PCL unit and carbon centres (2 and 4) substituted by isocyanate use to appear around 132–133 ppm while the unsubstituted carbon centres appear relatively in the upfield region, 121–122 ppm.

The aliphatic carbons including methyl group of TDI, ethyl group of PCL and other internal alkyl chain show their signals around 12–21 ppm and methylene carbons adjacent to oxygen centers and urethane units found to be noticed in the downfield range of 71–79 ppm due to the inductive effect [45]. The bottom NMR corresponds to the control PU, whereas the other two NMR spectra of PU-nanocomposite films (0.1% of SWCNTs and 0.3% of SWCNTs) are stacked to show the covalently bonded SWCNTs as tiny peak at 123 ppm is indicated by arrow in both spectra [46]. Such type of the tiny peak in solid state ^{13}C NMR has been already reported to confirm the presence of carbon nanotubes in nanocomposite materials [32].

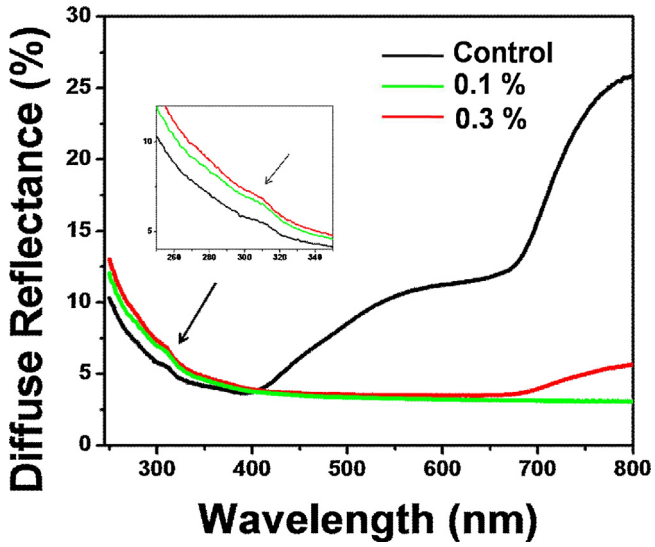

Fig. 8. UV–*vis* DRS spectra of PU control film and PU nanocomposite films.

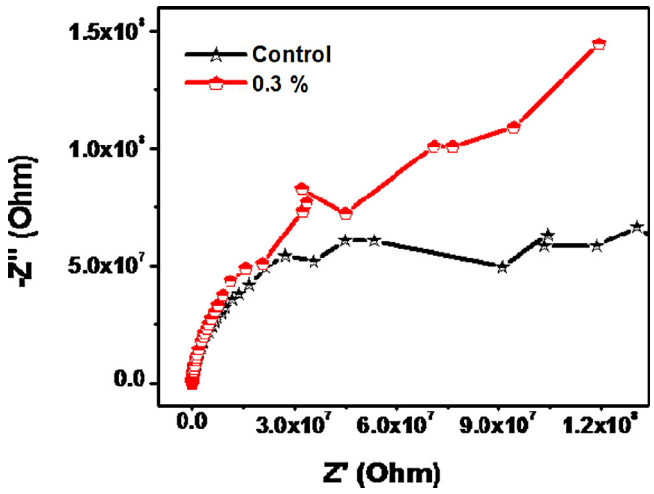

Fig. 9. Enhancement of conductivity based on SWCNTs loading (0.3 wt.%).

3.2.3. EDX analysis

XRD patterns of control PU film is shown in Fig. 5. The diffractogram deduce that the profile collected for this sample supposed to reveal amorphous characteristics with a broad diffraction band at $\Theta = 20.5^{\circ}$ and another shallow band around $\Theta = 43.16^{\circ}$. In particular, the pattern of peaks resembled with the data reported for the PU obtained from PCL with HDI [25].

EDX spectrum was collected for the control PU sample is shown in Fig. 5, which confirmed the presence of elemental composition such as carbon (42.35%), nitrogen (28.22%) and oxygen (29.43%) and supported the composition of the proposed polymeric network structure represented in Scheme 1. Some excessive low intensity peaks found in EDX data arisen due to the artefacts like sum peaks and escape peaks, also the detection of light elements (Be, B, C, N, O and F) undergo high absorption (lead to incorrect measurement of photons and shift in the peak position) based on their low photon energies [47,48].

3.2.4. Surface morphology and topography analysis

Optical microscopic images (Fig. S3 in SI) collected for the samples have encouraged us to study further by SEM to analyze the morphology of nanocomposite film homogeneously distributed with SWCNTs on PU matrix. SEM images shown in Fig. 6 supported the feature to be noted on the sample surface, which infer the widespread dispersion of $(OH)_n$-SWCNTs throughout the PU-SWCNTs nanocomposite film *i.e.*, interfacial network on film surface.

The bright lines were attributed to the SWCNTs that appear to be branched as rigid network without any agglomeration and fairly dark contrast region of surface specifies the polymer network, in which SWCNTs tend to established with proper interface. As such the fairly polar hydroxyl functionalized SWCNTs were noticed to be distributed uniformly free from any agglomeration around the PU network, whereas *p*-SWCNTs use to end up with agglomeration due to strong *Van der Walls* interaction and smaller dimension. Essentially the homogeneous suspension obtained by sonication of $(OH)_n$-SWCNTs in THF was used to obtain the formulation of nanocomposite films feasibly formed by covalent urethane bond in PU matrix [38].

Indeed, 3-dimensional AFM images in Fig. 7 were collected on the surface (probed at four different sites of film) to corroborate the topography of PU-SWCNTs nanocomposite (0.3 wt.%), which inferred the surface profile of PU network distributed with nanotubes. The height profile images for the above four images are depicted in Fig. S4 (SI). In panel of four images (A–D), the top two images (A and B) found to reveal grey and shiny regions consistently to support the distribution of SWCNTs. In the bottom images (C and D), the brighter regions correspond to the hard phase whereas the intense coloured regions represent the soft segments. Also the surface of this sample (A–D) comprised with concave regions due to the free motion of soft aliphatic polyester chains and the hard segments found to be slightly domed on different regions on surface [49,50].

3.2.5. Optical properties of PU and PU-SWCNTs nanocomposite films

Despite the interfacial interaction of $[OH]_n$-SWCNTs occur in PU nanocomposites, these films were noticed to exhibit appreciable transparency. However, the degree of transparency of PU nanocomposite films slightly reduced while increased the $[OH]_n$-SWCNTs loading (0.01%–0.3%).

Control PU film and PU-nanocomposites films (0.1 and 0.3%) were characterized by UV–vis diffuse reflectance spectra (DRS) to support the fact that these film samples are transparent in visible region as depicted in Fig. 8. The intensity of absorption maxima (λ_{max}) found to rise faintly at 310 nm for the nanocomposite films due to the minor increase in loading of SWCNTs into PU films as shown in the inset. In the UV region, the spectral profile of these three films occurred to reveal very minimum intensity among themselves, whereas the appreciable difference is observed between the control and nanocomposite films in the visible region. The intense peak in the visible region was identified for the control film in graph to support the maximum transparency of PU control film and no peak noticed in the visible region even upon trace loading of $[OH]_n$-SWCNTs (0.1 and 0.3%) in nanocomposite films [30–32].

3.2.6. Enhancement of electrical conductivity properties

Impedance spectroscopy data was collected to infer the conductivity of control PU and PU nanocomposites films of thickness (~1.5 mm), wherein real (Z') and imaginary (-Z'') values were used to plot in graph shown in Fig. 9. PU nanocomposite film (0.3 wt.% loading of $(OH)_n$-SWCNTs) found to exhibit the enhanced value in conductivity as compared to the control PU film. The conductivity value has increased about one order due to the covalent addition of SWCNTs. Despite the above study was conducted with the biodegradable nanocomposite film loaded with minor loading of SWCNTs (0.3 wt.%), the magnitude of increase in conductivity value

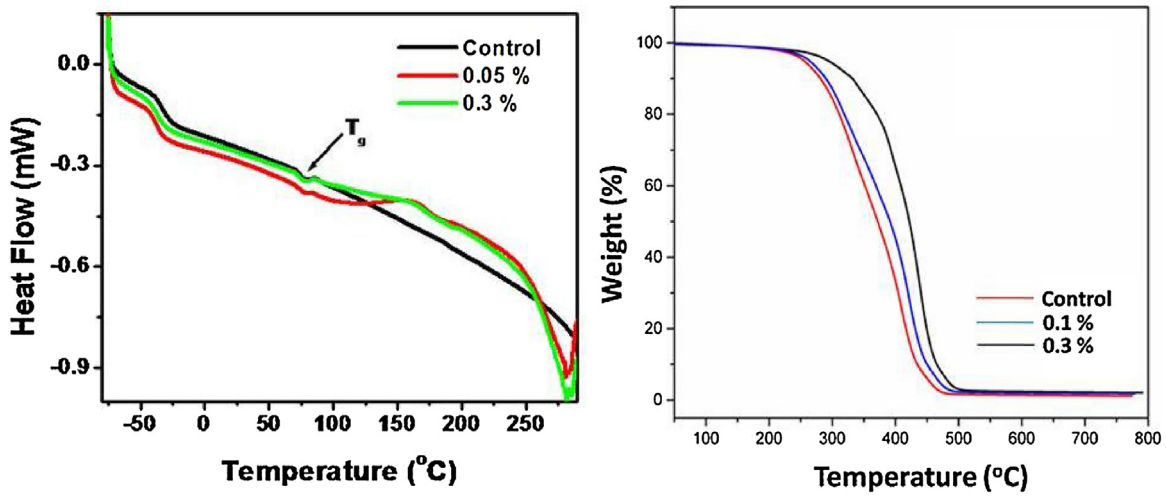

Fig. 10. (a) DSC profile of data of PU and PU-SWCNTs nanocomposite films, (b) TGA thermograms of PU and PU-SWCNTs nanocomposite films.

suggested its potential contribution in terms of electrical characteristics [23,24,32].

3.2.7. Enhancement of thermal properties

Both DSC and TGA studies were conducted to characterize the thermal properties of these samples. DSC profiles obtained for the samples, control PU and PU nanocomposites with loadings, 0.1 and 0.3 wt.% were compared in Fig. 10a. Single T_g value has been noticed for the control film at 77 °C, whereas the PU-SWCNTs samples containing 0.1 wt.% of SWCNTs as well as 0.3 wt.% of SWCNTs were noted to appear at 77 °C and no variation observed while compared between control and nanocomposite samples. Despite there is no variation of T_g value of PU against PU nanocomposite samples, appreciable shift in T_g value is noticed with DSC profile as compared to their polyol precursor, PCL (T_g = 44.9 °C) depicted in Fig. S5. Moreover, DSC profile did not show any melting peak with any of these samples up to 250 °C, indicating the thermal stability of the PU and nanocomposite samples [32].

Thermal characterization by TGA provided information on the potential improvement in thermal stability due to the addition of SWCNTs. TGA profile of the selective samples are shown in Fig. 10b, wherein degradation occurred in single step with onset degradation temperature above 430 °C while examined on these film samples. Despite the minor loadings of SWCNTs achieved by covalent incorporation into PU matrix, enhancement in thermal stability (0.1 wt.%: 448 °C and 0.3 wt.%: 462 °C) has been observed as appreciable shift in degradation temperature as compared to the control sample (433 °C). Altogether nanocomposite samples exhibit the desired variation in degradation temperature, as shown in Fig. 10b. Thermal studies exhibited the improvement in thermal conductivity due to the facilitation of heat transport by SWCNTs, lead to incorporation of thermal stability on nanocomposite films due to the uniform dispersion of SWCNTs incurred in PU matrix [25–27,51].

3.2.8. Mechanical properties of PU nanocomposite films

Mechanical properties for the control PU and PU-SWCNTs composite film samples have been measured and entered in Table 1. Essentially, the tensile strength of control PU and PU-SWCNTs nanocomposite films (0.05, 0.1 and 0.3%) were measured to identify the enhancement of tensile strength due to the incorporation of $(OH)_n$-SWCNTs into the PU matrix. In fact the tensile strength of PU depends on the chemical composition and nature of the soft and hard segment used in formulation [52]. PU samples tend to exhibit

Table 1
Tensile strength of PU and PU nanocomposite films at different loading.

S. No.	Sample	Tensile strength (N/mm^2)	Elongation at Break (%)
1.	Control PU	4.01	190.75
2.	0.05%	4.16	116.70
3.	0.1%	4.30	116.25
4.	0.3%	5.01	154.40

better tensile strength and lesser elongation at break while increasing the hard segment of the composition. Mechanical tests of PU developed from PCL and HDI found to reveal the flexible behaviour in polyurethane films, tensile strength value was 3.6 MPa [53]. The stoichiometric proportion of rigid and reactive hard segment reagent, TDI has been chosen to obtain the control PU with better tensile strength, 4.01 MPa. The interfacial interaction of SWCNTs in PU network enhanced the tensile strength of nanocomposite films, as inferred from the gradational increase in its tensile strength value from 3.8–25.0% while varied loading between 0.05–0.3 wt.%. Tensile values in entry 3 and 4 were deduced to exhibit the increase in plastic behavior, since the stress-strain curve pass through the strain hardening region, which is above the steady state and critical stress [2,32,54].

4. Conclusions

Since we aim to develop the biodegradable PU samples, major component of trifunctional polyol, PCL (approximately 70%) has been taken with TDI in the presence of PMDETA to synthesize PU, without addition of tin catalyst. PU matrix was transformed to film (~1.5 mm) by casting approach and hydroxyl functionalized single-walled carbon nanotubes [$(OH)_n$-SWCNTs] occurred to synthesize from *p*-SWCNTs by simple and mild synthetic route to exclude the conventional and rigorous condition. The insoluble PU film samples were obtained upon *in situ* covalent addition of trace quantity of [$(OH)_n$-SWCNTs] into PU matrix followed by film casting protocol. Also physicochemical characteristics were studied to support the proposed 3-dimensional structural network of PU as well as the covalent addition SWCNTs into PU. Despite the PU possess biodegradable structure with minor quantity of SWCNTs (0.01–0.3%), tend to reveal fair enhancement in electrical, thermal and mechanical properties based on the influence of SWCNTs. The uniform dispersion and interfacial interaction of SWCNTs

in PU matrix has been identified from the morphological images and enhancement other characteristic properties. This work provides an insight towards the scope to choose the biodegradable PU matrix as candidate for generating PU nanocomposites as prospective as that of other reported non-degradable polymeric samples formulated from the conventional petro-based resources.

Acknowledgements

The first author (GTSA) sincerely thanks the Council of Scientific and Industrial Research (CSIR), New Delhi, India for the Quick Hire Scientist fellowship. Also we thank Perstrop India Limited for gifted the polyol (CAPA 3201) sample.

Appendix A. Supplementary data

Supplementary data associated with this article can be found, in the online version, at https://doi.org/10.1016/j.apsusc.2018.01.275.

References

[1] N.G. Sahoo, S. Rana, J.W. Cho, L. Li, S.H. Chan, Polymer nanocomposites based on functionalized carbon nanotubes, Prog. Polym. Sci. 35 (2010) 837–867.
[2] S.A. Gurusamy-Thangavelu, S.J. Emond, A. Kulshrestha, M.A. Hillmyer, C.W. Macosko, W.B. Tolman, T.R. Hoye, Polyurethanes based on renewable polyols from bioderived lactones, Polym. Chem. 3 (2012) 2941–2948.
[3] S. Thakur, N. Karak, Bio-based tough hyperbranched polyurethane–graphene oxide nanocomposites as advanced shape memory materials, RSC Adv. 3 (2013) 9476–9482.
[4] M.A. Hillmyer, W.B. Tolman, Aliphatic polyester block polymers: renewable, degradable, and sustainable, Acc. Chem. Res. 47 (2014) 2390–2396.
[5] S.S. Bari, A. Chatterjee, S. Mishra, Biodegradable polymer nanocomposites: an overview, Polym. Rev. 56 (2016) 287–328.
[6] A. Murali, S.A. Gurusamy-Thangavelu, S.N. Jaisankar, A.B. Mandal, Enhancement of the physicochemical properties of polyurethane–perovskite nanocomposites via addition of nickel titanate nanoparticles, RSC Adv. 5 (2015) 102488–102494.
[7] H. Tian, Z. Tang, X. Zhuang, X. Chen, X. Jing, Biodegradable synthetic polymers: preparation: functionalization and biomedical application, Prog. Polym. Sci. 37 (2012) 237–280.
[8] A. Muñoz-Bonilla, M.L. Cerrada, M. Fernández-García, A. Kubacka, M. Ferrer, M. Fernández-García, Biodegradable polycaprolactone-titania nanocomposites: preparation: characterization and antimicrobial properties, Int. J. Mol. Sci. 14 (2013) 9249–9266.
[9] D. Thomas, J.J. Cabibihan, S. Kumar, S.K. Pasha, D. Mandal, M. Laad, B.C. Yadav, S.I. Patil, A. Ghule, P. Mazumdar, S. Rattan, Biodegradable nanocomposites for energy harvesting, self-healing, and shape memory, in: Smart Polymer Nanocomposites, Springer International Publishing, 2017, pp. 377–397.
[10] D. Depan (Ed.), Biodegradable Polymeric Nanocomposites: Advances in Biomedical Applications, CRC Press, 2015.
[11] M. Labet, W. Thielemans, Synthesis of polycaprolactone: a review, Chem. Soc. Rev. 38 (12) (2009) 3484–3504.
[12] Z. You, X. Bi, E.M. Jeffries, Y. Wang, A biocompatible: metal-free catalyst and its application in microwave-assisted synthesis of functional polyesters, Polym. Chem. 3 (2012) 384–389.
[13] A. Marcos-Fernández, G.A. Abraham, J.L. Valentín, J. San Román, Synthesis and characterization of biodegradable non-toxic poly (ester-urethane-urea) s based on poly (ε-caprolactone) and amino acid derivatives, Polymer 47 (2006) 785–798.
[14] A. Palanisamy, M.S.L. Karuna, T. Satyavani, D.R. Kumar, Development and characterization of water-blown polyurethane foams from diethanolamides of karanja oil, J. Am. Oil Chem. Soc. 88 (2011) 541–549.
[15] N. Karak, Biobased smart polyurethane nanocomposites: from synthesis to applications, R. Soc. Chem. 26 (2017).
[16] R.C.M. Dias, A.M. Góes, R. Serakides, E. Ayres, R.L. Oréfice, Porous biodegradable polyurethane nanocomposites: preparation, characterization, and biocompatibility tests, Mater. Res. 13 (2010) 211–218.
[17] W. Chen, X. Tao, Production and characterization of polymer nanocomposite with aligned single wall carbon nanotubes, Appl. Surf. Sci. 252 (2006) 3547–3552.
[18] L.H. Chan-Chan, R. Solis-Correa, R.F. Vargas-Coronado, J.M. Cervantes-Uc, J.V. Cauich-Rodríguez, P. Quintana, P. Bartolo-Pérez, Degradation studies on segmented polyurethanes prepared with HMDI: PCL and different chain extenders, Acta Biomater. 6 (2010) 2035–2044.
[19] D. Eyrich, H. Wiese, G. Maier, D. Skodacek, B. Appel, H. Sarhan, J. Tessmar, R. Staudenmaier, M.M. Wenzel, A. Goepferich, T. Blunk, In vitro and in vivo cartilage engineering using a combination of chondrocyte-seeded long-term stable fibrin gels and polycaprolactone-based polyurethane scaffolds, Tissue Eng. 13 (2007) 2207–2218.
[20] B.R. Barrioni, S.M. de Carvalho, R.L. Oréfice, A.A.R. de Oliveira, M. de Magalhães Pereira, Synthesis and characterization of biodegradable polyurethane films based on HDI with hydrolyzable crosslinked bonds and a homogeneous structure for biomedical applications, Mater. Sci. Eng.: C 52 (2015) 22–30.
[21] S. Iijima, Helical microtubules of graphitic carbon, Nature 354 (1991) 56–58.
[22] M.C. Hersam, Progress towards monodisperse single-walled carbon nanotubes, Nat. Nanotechnol. 3 (2008) 387–394.
[23] I. Alig, P. Pötschke, D. Lellinger, T. Skipa, S. Pegel, G.R. Kasaliwal, T. Villmow, Establishment: morphology and properties of carbon nanotube networks in polymer melts, Polymer 53 (2012) 4–28.
[24] R. Zhang, A. Dowden, H. Deng, M. Baxendale, T. Peijs, Conductive network formation in the melt of carbon nanotube/thermoplastic polyurethane composite, Compos. Sci. Technol. 69 (2009) 1499–1504.
[25] P.M. Ajayan, L.S. Schadler, C. Giannaris, A. Rubio, Adv. Mater. 12 (2000) 750.
[26] P. Singh, S. Campidelli, S. Giordani, D. Bonifazi, A. Bianco, M. Prato, Organic functionalisation and characterisation of single-walled carbon nanotubes, Chem. Soc. Rev. 38 (2009) 2214–2230.
[27] D. Samanta, R.M. Sankar, S.N. Jaisankar, M.S. Alam, A.B. Mandal, Acid-responsive microcapsules: the loading–unloading processes, Chem. Commun. 47 (2011) 11975–11977.
[28] R.H. Baughman, A.A. Zakhidov, W.A. De Heer, Carbon nanotubes–the route toward applications, Science 297 (2002) 787–792.
[29] C. Sanchez, P. Belleville, M. Popall, L. Nicole, Applications of advanced hybrid organic–inorganic nanomaterials: from laboratory to market, Chem. Soc. Rev. 40 (2011) 696–753.
[30] H. Xia, M. Song, Preparation and characterization of polyurethane?carbon nanotube composites, Soft Matter 1 (2005) 386–394.
[31] H. Xia, M. Song, Preparation and characterisation of polyurethane grafted single-walled carbon nanotubes and derived polyurethane nanocomposites, J. Mater. Chem. 16 (2006) 1843–1851.
[32] A. Murali, S.A. Gurusamy-Thangavelu, S.N. Jaisankar, A.B. Mandal, Augmentation of properties on sparingly loaded nanocomposites via functionalized single-walled carbon nanotubes using a covalent approach, RSC Adv. 4 (2014) 62947–62950.
[33] M. Raja, S.H. Ryu, A.M. Shanmugharaj, Thermal: mechanical and electroactive shape memory properties of polyurethane (PU)/poly (lactic acid)(PLA)/CNT nanocomposites, Eur. Polym. J. 49 (2013) 3492–3500.
[34] Y.C. Jung, N.G. Sahoo, J.W. Cho, Polymeric nanocomposites of polyurethane block copolymers and functionalized multi-walled carbon nanotubes as crosslinkers, Macromol. Rapid Commun. 27 (2) (2006) 126–131.
[35] D.B. Mawhinney, V. Naumenko, A. Kuznetsova, J.T. Yates, J. Liu, R.E. Smalley, Infrared spectral evidence for the etching of carbon nanotubes: ozone oxidation at 298 K, J. Am. Chem. Soc. 122 (2000) 2383–2384.
[36] A. Hirsch, Functionalization of single-walled carbon nanotubes, Angew. Chem. Int. Ed. 41 (2002) 1853–1859.
[37] M. Krishnamurthy, K. Krishnamoorthy, A. Arulkashmir, V. Raghavendra, A. Murali, S.N. Jaisankar, P. Murugan, S.A. Gurusamy-Thangavelu, A.S. Nasar, A.B. Mandal, D. Samanta, Click polymerization: a convenient strategy to prepare designer fullerene materials, Mater. Des. 108 (2016) 34–41.
[38] D.J. Nelson, H. Rhoads, C. Brammer, Characterizing covalently sidewall-functionalized SWNTs, J. Phys. Chem. C 111 (2007) 17872–17878.
[39] H. Pan, L. Liu, Z.X. Guo, L. Dai, F. Zhang, D. Zhu, R. Czerw, D.L. Carroll, Carbon nanotubols from mechanochemical reaction, Nano Lett. 3 (2003) 29–32.
[40] M.A. Kabbani, C.S. Tiwary, P.A. Autreto, G. Brunetto, A. Som, K.R. Krishnadas, S. Ozden, K.P. Hackenberg, Y. Gong, D.S. Galvao, R. Vajtai, Ambient solid-state mechano-chemical reactions between functionalized carbon nanotubes, Nat. Commun. 6 (2015) 1–8.
[41] J. Chen, M.A. Hamon, H. Hu, Y. Chen, A.M. Rao, P.C. Eklund, R.C. Haddon, Solution properties of single-walled carbon nanotubes, Science 282 (1998) 95–98.
[42] F. Hennrich, R. Krupke, S. Lebedkin, K. Arnold, R. Fischer, D.E. Resasco, M.M. Kappes, Raman spectroscopy of individual single-walled carbon nanotubes from various sources, J. Phys. Chem. B 109 (2005) 10567–10573.
[43] S. Parnell, K. Min, M. Cakmak, Kinetic studies of polyurethane polymerization with Raman spectroscopy, Polymer 44 (2003) 5137–5144.
[44] R.N. Jana, H.J. Yoo, J.W. Cho, Synthesis and properties of shape memory polyurethane nanocomposites reinforced with poly (ε-caprolactone)-grafted carbon nanotubes, Fibers Polym. 9 (2008) 247–254.
[45] T.L. Wang, F.J. Huang, S.W. Lee, Preparation and characterization of star polymers with polyurethane cores using polycaprolactone triol, Polym. Int. 51 (2002) 1348–1352.
[46] C. Engtrakul, M.F. Davis, K. Mistry, B.A. Larsen, A.C. Dillon, M.J. Heben, J.L. Blackburn, Solid-state 13C NMR assignment of carbon resonances on metallic and semiconducting single-walled carbon nanotubes, J. Am. Chem. Soc. 132 (2010) 9956–9957.
[47] J.I. Goldstein, D.E. Newbury, J.R. Michael, N.W. Ritchie, J.H.J. Scott, D.C. Joy, Scanning Electron Microscopy and X-ray Microanalysis, Springer, 2017.
[48] D.E. Newbury, Mistakes encountered during automatic peak identification of minor and trace constituents in electron-excited energy dispersive X-ray microanalysis, Scanning 31 (2009) 91–101.
[49] C.H. Lee, J.Y. Liu, S.L. Chen, Y.Z. Wang, Miscibility and properties of acid-treated multi-walled carbon nanotubes/polyurethane nanocomposites, Polym. J. 39 (2007) 138–146.

[50] B. Gong, C. Ouyang, Y. Yuan, Q. Gao, Synthesis and properties of a millable polyurethane elastomer with low halloysite nanotube content, RSC Adv. 5 (2015) 77106–77114.
[51] Q. Jing, J.Y. Law, L.P. Tan, V.V. Silberschmidt, L. Li, Z. Dong, Preparation: characterization and properties of polycaprolactone diol-functionalized multi-walled carbon nanotube/thermoplastic polyurethane composite, Compos. Part A: Appl. Sci. Manuf. 70 (2015) 8–15.
[52] M. Szycher (Ed.), Szycher's Handbook of Polyurethanes, CRC Press, 2012.
[53] B.R. Barrioni, S.M. de Carvalho, R.L. Oréfice, A.A.R. de Oliveira, M. de Magalhães Pereira, Synthesis and characterization of biodegradable polyurethane films based on HDI with hydrolyzable crosslinked bonds and a homogeneous structure for biomedical applications, Mater. Sci. Eng.: C 52 (2015) 22–30.
[54] T.E. Tullis, J. Tullis, Experimental rock deformation techniques, Mine. Rock Deform.: Lab. Stud.: Paterson Vol. (1986) 297–324.